Vol 14 No 12, December 2005
1009-1963/2005/14(12)/2529-10
Chinese Physics
© 2005 Chin. Phys. Soc.
and IOP Publishing Ltd

Orientation distribution of fibres in a channel flow of fibre suspension*

Lin Jian-Zhong(林建忠)[a)†], Li Jun(李 俊)[a)], and Zhang Wei-Feng(张卫峰)[b)]

[a)] *Department of Mechanics, State Key Laboratory of Fluid Power Transmission and Control, Zhejiang University, Hangzhou 310027, China*

[b)] *Institute of Marine and Coastal Sciences, Rutgers University, New Brunswick, New Jersey, 08903-0231*

(Received 25 April 2005; revised manuscript received 24 July 2005)

The orientation and concentration distributions of fibres in laminar and turbulent channel flows are investigated numerically. The obtained results are in good agreement with the experimental data. In the laminar flow regime, more fibres orient to the flow direction as the Reynolds number increases. The shear rate of fluid around a fibre plays an important role in determining the orientation distribution of fibres, while the fibre density and the fibre aspect-ratio have marginal influence on the orientation distribution. In the turbulent regime, the orientation distribution of fibres becomes more homogeneous with the increase of Reynolds number, and the concentration profile is flatter than that in the laminar regime. The fluctuating intensity of fibre velocity in the downstream direction is larger than that in the lateral directions.

Keywords: fibres, orientation, concentration, channel flow, numerical simulation
PACC: 4755K, 4750, 4725J, 4760

1. Introduction

The investigation of particle transport processes has attracted considerable attention due to their numerous industrial and practical applications.[1] Pneumatic transport, air pollution and microcontamination are among the areas in which the knowledge of particle dispersion plays a critical role. The currently available literature of particle dispersion is exclusively concerned with idealized spherical particles, however, in reality natural dust and industrial solid particles are all nonspherical. The motions of nonspherical particles in flows are much complicated because the rotational motion is strongly coupled with the translation motion.

Fibre is a kind of nonspherical particles and has been a subject of extensive investigation, for example, the diffusivity constant, the structure functions, and the reduced viscosity of fibre suspensions were examined numerically by Fan *et al*[2] Feng and Leal[3] explored the mechanisms for the generation of disclinations in a non-homogeneous flow and studied the coupling between the flow and the polymer configuration. Recently Lin *et al*[4] conducted the investigation on the spatial and orientation distributions of fibres in an evolving mixing layer numerically and experimentally.

The characterization of fibre suspensions in a channel is of scientific interest and important in many industrial processes.[5] The channel flow is the flow that has a main direction within two planes; the fluid flows into inlet and after travelling a definite distance from the inlet it becomes full-developed, with a velocity profile being different for lamina and turbulent states. Nsom[6] reported the results of the drag reduction phenomenon in dilute and semi-concentrated fibre suspensions in a wide-gap Couette–Taylor configuration. Chiba *et al*[7] computed the coupled flow kinematics and fibre orientation distribution, and obtained the anisotropic characteristics of fibre orientations and stress field in the region near the inlet. Yasuda *et al*[8] used a new visualization technique to observe the fibre orientation, fibre concentration distribution and the relationship between total shear strain and orientation angle. You *et al*[9] presented a linear

*Project supported by the National Natural Science Foundation (Grant No 10372090) and the Doctorate Program of Higher Education of China (Grant No 20030335001).
†Corresponding author: E-mail: jzlin@sfp.zju.edu.cn

instability analysis of the channel flow in the presence of fibre additives, and found that the flow instability of fibre suspensions was governed by two parameters: a ratio of the axial stretching resistance of fibres to the inertial force of the fluid, and the orientational diffusivity coefficient that accounts for inter-fibre hydrodynamic interactions. The increase in either of the above two parameters causes an increase in critical Reynolds number, i.e. the fibre suspensions become more stable. Olson *et al*[10] proposed an Eulerian model of turbulent fibre suspensions flowing through a planar contraction to predict the fibre orientation distribution, and applied the model specifically to the flow of pulp suspensions through a papermachine headbox. It was demonstrated that with the increase of the contraction ratio the alignment of fibres exiting from the headbox significantly increased, and varying the inlet fluid velocity could only cause small changes in the fibre orientation distribution.

The mechanical properties of fibre reinforced plastics greatly depend on the fibre orientation and its concentration distribution. Under most circumstances, fibre processing is performed at a high rate in turbulent flows. Up to now, the effects of Reynolds number, shear rate of fluid, fibre aspect-ratio and fibre density on the orientation and concentration distributions of fibres in both laminar and turbulent flows appear to be an unexplored topic of research. Therefore, this study aims at giving the information mentioned above by simulating numerically the motion of fibres in laminar and turbulent channel flows with the Lagrangian model.

2. Background flow

2.1. Mean velocity

The background flow is a channel flow, as shown in Fig.1. In order to simulate the motion of fibres, the flow field should be known beforehand. For a laminar flow, we can obtain the analytic solution for the velocity

$$u_z = \frac{3}{2} u_{\rm av} \left(1 - \frac{r^2}{H^2}\right), \qquad (1)$$

where u_z is the downstream velocity, H is the half width of channel, r is the distance to the centre line, $u_{\rm av}$ is the average velocity of flow. For a turbulent flow, we have the following mean velocity profile:

$$\frac{\overline{u}_z}{u^*} = 5.75 \lg \frac{u^*(H-r)}{\nu} + 5.5, \quad \overline{u}_r = 0, \qquad (2)$$

where u^* is the wall friction velocity and defined by $\sqrt{\tau_{\rm w}/\rho}$, $\tau_{\rm w}$ is the wall friction, ν is the viscosity of fluid.

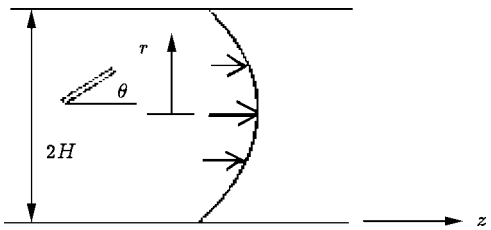


Fig.1. Channel flow.

2.2. Fluctuating velocity

Equation (2) describes the mean velocity; we should give the turbulent velocity further in the turbulent flows. In the majority of applications, the characteristic length scale of fibres is less than 1 mm and smaller than the turbulent Kolmogoroff's length scale (larger than 1 mm at least). Thus, the fluctuating velocity of fluid plays an important role in the motion of fibres and is required to simulate the motion of each fibre.

Because the random drive of flow on fibres is what we only want to obtain, a stochastic simulation method is employed here. Wang and Stock[11] generated numerically a turbulent flow in Fourier modes and an appropriate expression of one point velocity correlation and scalar energy spectrum. A KSSM (Kinetic Simulation Sweeping Model) was developed to simulate the dynamical interactions between different modes (e.g. vortex stretching) and the kinematic process of non-uniform unsteady advection of the vorticity field by the velocity field in homogeneous isotropic turbulence.[12]

Here, we combine these two methods to develop a modified method and then apply the modified method to the turbulent channel flow. The fluctuating velocity field of fluid, $\boldsymbol{u}'$, can be represented with a Fourier series as follows:

$$\frac{\boldsymbol{u}'(\boldsymbol{x},t)}{\boldsymbol{u}_{\rm rms}(\boldsymbol{x})} = \sum_{n=1}^{N} [(\boldsymbol{b}_n \times \boldsymbol{k}_n)\cos(\boldsymbol{k}_n \cdot \boldsymbol{x} - \omega_n t) + (\boldsymbol{c}_n \times \boldsymbol{k}_n)\sin(\boldsymbol{k}_n \cdot \boldsymbol{x} - \omega_n t)]. \qquad (3)$$

Here, N is a big constant (N=100 in this paper), $\boldsymbol{b}_n$ and $\boldsymbol{c}_n$ are vectors composed of Gaussian random numbers, frequency ω_n is also the Gaussian random number whose standard deviation is the RMS (root-mean-square) of fluctuating velocity, $\boldsymbol{u}_{\rm rms}$, and wave

number vector, $\boldsymbol{k}_n$, is the isotropic unit random vector. Therefore, the dot product of the coefficient of primary function and the wave number vector is zero $((\boldsymbol{b}_n \times \boldsymbol{k}_n) \cdot \boldsymbol{k}_n = 0)$, which ensures the flow field being incompressible.

Through systematic experiments on the turbulent channel flow, Comte-Bellot[13] obtained the distribution of $\boldsymbol{u}_{\rm rms}$ on the channel cross-section at different Reynolds numbers. ω_n and the components of $\boldsymbol{b}_n$, $\boldsymbol{c}_n$ and $\boldsymbol{k}_n$ can be determined from $\boldsymbol{u}_{\rm rms}$. Then, the fluctuating velocity, $\boldsymbol{u}'(x,t)$, can be computed from Eq.(3). Adding the fluctuating velocity to the mean velocity yields the instantaneous velocity.

Figure 2 gives a comparison of the components of relative turbulent intensity as a function of lateral distance with the measurements given by Comte-Bellot. The computational results are in good agreement with the measurements. Both of them show that the relative turbulent intensities are weaker at a position closer to the centre of channel. We can see that the results obtained with the simplified simulation method in this paper reflect the characteristics of the second-order correlations in the real turbulent flow. Therefore, we conclude that the simplified simulation method is able to produce reasonable results.

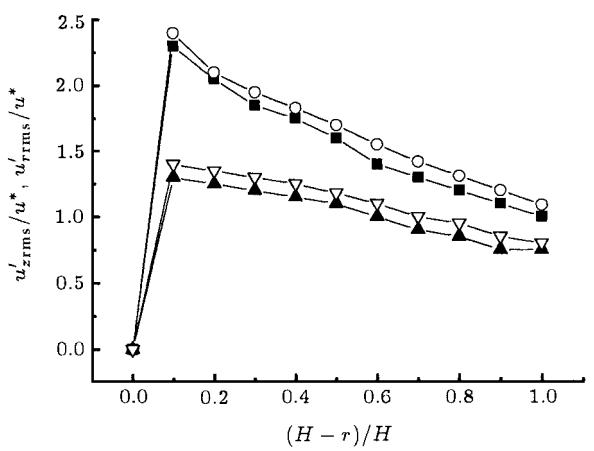


Fig.2. Distribution of relative turbulent intensities versus lateral position. —○—: computation of $\sqrt{\overline{u'^2_z}}/u^*$ in this paper; — ■ —: Comte-Bellot's experimental data of $\sqrt{\overline{u'^2_z}}/u^*$; —▽—: computation of $\sqrt{\overline{u'^2_r}}/u^*$ in this paper; — ▲ —: Comte-Bellot's experimental data of $\sqrt{\overline{u'^2_r}}/u^*$.

3. Description of fibre suspensions

3.1. Basic assumptions

Generally there are two approaches to simulating fibre suspensions: Eulerian method and Lagrangian method. For the former, the constitutive equation including the effects of particle–particle[14,15] and particle–solvent[16] should be considered. The Lagrangian method used in the present study is usually employed to predict the spatial and orientation distributions of fibres in the dilute or semi-dilute fibre suspensions. The fibre in simulation is shown in Fig.3. The computations are based on the following general assumptions:

(1) The continuous medium hypothesis is suitable, i.e. $Kn << 1$.

(2) Fibres are non-Brownian, slender rigid cylinders in Newtonian fluid and the aspect-ratio is large, $l/a >> 1 (l, a$ are the half length and the radius of the fibre respectively), and the end effect of cylinders is not considered.

(3) The length of fibre is much smaller than that of the flow field and smaller than the mesh size as well, so that the flow around each fibre can be considered as the Stokes flow.

(4) The suspension is dilute, and the interactions among the fibres and the lubrication effects can be neglected.

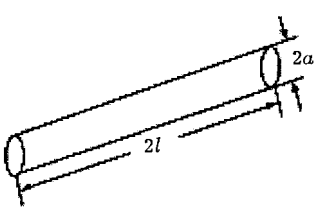


Fig.3. Fibre particle.

3.2. Description of fibre motion

Based on the above assumptions, Batchelor[17] established the slender-body theory of which the main principle is that the disturbance motion resulting from the presence of the slender body is approximately the same as that due to a suitably chosen line distribution of Stokeslets. A Stokeslet is a singularity in Stokes flow representing the effect of a force exerted on the fluid at a point.

From the Stokes equation, we can obtain the following expressions of the induced velocity of a point force on fluid:[18]

$$\boldsymbol{u}(\boldsymbol{x}) = \boldsymbol{F} \cdot \frac{\boldsymbol{G}(\boldsymbol{x})}{8\pi\mu}, \tag{4}$$

where μ is the viscosity of fluid, $\boldsymbol{F}$ is the force on a fibre, $\boldsymbol{G}(\boldsymbol{x})$ is the Green tensor:

$$G_{ij} = \frac{1}{r}\delta_{ij} + \frac{1}{r^3}x_i x_j. \tag{5}$$

After the integration along the fibre and the simplification in the slender body approximation, the induced velocity caused by the existence of fibre can be obtained:[19]

$$\begin{aligned}\boldsymbol{V} =& \boldsymbol{u}^{\infty}(\boldsymbol{x}_c + ls\boldsymbol{p}) - [\boldsymbol{U} + (\omega \times ls\boldsymbol{p})] \\ =& -2\left(\ln 2\beta + \ln\frac{\sqrt{1-s^2}}{b(s)}\right)(\boldsymbol{\delta} + \boldsymbol{pp})\cdot\boldsymbol{f}(s) \\ & -(\boldsymbol{\delta} - 3\boldsymbol{pp})\cdot\boldsymbol{f}(s) - (\boldsymbol{\delta} + \boldsymbol{pp}) \\ & \cdot\int\frac{\boldsymbol{f}(s) - \boldsymbol{f}(s')}{|s - s'|}\mathrm{d}s',\end{aligned} \tag{6}$$

where $\boldsymbol{\omega}$ is the angular velocity of fibre, $\boldsymbol{p}$ the orientation vector of fibre, s the nondimensional length coordinate of fibre with $-1 \le s \le 1$, $\boldsymbol{\delta}$ the unit matrix, U the translational velocity of fibre, $\boldsymbol{u}^{\infty}$ the undisturbed flow velocity, $\boldsymbol{x}_c$ the coordinate of fibre mass centre, $b(s)$ the shape factor of cross-section with coordinate s, ($b(s) = 1$ for fibre), and $\boldsymbol{f}(s)$ the force acting on the fibre by fluid. The left-hand side of the Eq.(6) is the velocity difference between fibre and fluid at a position s, while the terms on the right-hand side result in this velocity difference because of the existence of fibre. We can use Eq.(6) to compute the motion of fibres. In the equation, $\boldsymbol{f}(s)$ is unknown. The fibre can be divided into M segments according to the Gauss integral point (M=10 in this paper), then $\boldsymbol{f}(s)$ is transferred to $\boldsymbol{f}(s_i)$ on each segment, there are $3M$ unknown numbers altogether. Next the integration on the right-hand side of Eq.(6) can be transferred into linear summation of a series of $\boldsymbol{f}(s_i)$. In the computation, the velocity, angular velocity of fibre and velocity of fluid at a definite time are known, so the velocity difference on the left-hand side of Eq.(6) is known. Thus, Eq.(6) can be transformed into a system of linear equations which includes $3M$ equations:

$$\boldsymbol{b}_i = \boldsymbol{A}_i\cdot\boldsymbol{f}(s_i) + t_i\boldsymbol{B}\cdot\boldsymbol{f}(s_i) - \sum_{\substack{m=1\\m\neq i}}^{M} k_{im}\boldsymbol{B}\cdot\boldsymbol{f}(s_m),$$

$$(i = 1, 2, \cdots, M), \tag{7}$$

where

$$\boldsymbol{b}_i = \boldsymbol{u}^{\infty}(\boldsymbol{x}_c + ls_i\boldsymbol{p}) - [\boldsymbol{U} + (\omega \times ls_i\boldsymbol{p})],$$

$$\boldsymbol{A}_i = 2(\ln 2\beta + \ln\sqrt{1 - \boldsymbol{s}_i^2})(\boldsymbol{\delta} + \boldsymbol{pp}) + (\boldsymbol{\delta} - 3\boldsymbol{pp}),$$

$$B = (\boldsymbol{\delta} + \boldsymbol{pp}),\quad t_i = \sum_{\substack{m=1\\m\neq i}}^{M}\frac{l_m}{|s_i - s_m|},\quad k_{im} = \frac{l_m}{|s_i - s_m|}.$$

We obtain $\boldsymbol{f}(s_i)$ by solving Eq.(7), then the total force and total moment acting on the fibre respectively are

$$\boldsymbol{F} = 8\pi\mu l\int_{-1}^{1}\boldsymbol{f}(s)\mathrm{d}s,$$

$$\boldsymbol{L} = 8\pi\mu l^2\int_{-1}^{1}s\boldsymbol{p}\times\boldsymbol{f}(s)\mathrm{d}s. \tag{8}$$

Equation (8) can be solved by numerically integrating to obtain the total force and total moment. Then, Newton's second law and the 3D rotational equation of fibre

$$m\frac{\mathrm{d}\boldsymbol{U}}{\mathrm{d}t} = \boldsymbol{F},\quad \boldsymbol{J}_{\mathrm{c}}\cdot\frac{\mathrm{d}\boldsymbol{\omega}}{\mathrm{d}t} + \boldsymbol{\omega}\times\boldsymbol{J}_{\mathrm{c}}\cdot\boldsymbol{\omega} = \boldsymbol{L}. \tag{9}$$

are used to calculate the acceleration and angular acceleration. Finally, the velocity, angular velocity, position, orientation vector of fibre can be computed with the finite difference method.

4. Results and discussion

Because we have not found any published literature about orientation distribution of fibres in the channel flows, the corresponding results in the pipe flow given by Bernstein and Shapiro[20] are used for comparison with the computational results. The channel flow is a two-dimensional flow while the pipe flow is an axis-symmetric flow. Though the cross sections are different for these two flows, their distributions of velocity and turbulent quantities from wall to centre are very similar. Therefore, the parameter values selected in our computations are similar to those in the experiments. The channel width is 50 mm, the fluid is water with a density of 1000kg/m^3 at a temperature of 300K, and a viscosity of 8.55×10^{-4}N·s/m^2. Fibres with a density of 2000kg/m^3 are initially distributed randomly in the exit of channel. The initial translational velocity and angular velocity for each fibre are both zero. The initial computation time step is $10^{-11} - 10^{-10}$s. The orientation distributions of fibres are obtained statistically within a rectangular region with 50 mm (channel width) $\times$30 mm (along flow direction).

4.1. The effect of Re number on the orientation distribution of fibres in the laminar flows

Figure 4 plots the orientation distribution of fibres in terms of θ for different Re, which is based

on the fluid average velocity and the channel width. Figure 5 shows the relationship between the mean orientation θ and Re number. From the figures, we can see that the computational and experimental results are in qualitative agreement. Some deviations may result from the difference between the two flows. At a low Re, the fibre orientation is less dependent on θ and seems equally possible in all directions, and with Re increasing, the fibres' orientation to the flow direction becomes more obvious, which is also shown in Fig.5. For our numerical model, the fluid inertia is not considered, i.e. $\mathrm{Re_p}$=0 ($\mathrm{Re_p} = lu_\mathrm{d}/\nu$, where l is the length of fibre, u_d is the difference in velocity between fluid and fibre, ν is the viscosity of fluid), and fibres rotate in the flow-gradient plane. According to the theory of Jeffrey orbit, the motion of fibres can be determined by their initial orientation if the flow is a simple shear flow. However, the particle inertia is taken into account in this paper, and the flow is not exactly simple shear flow, these two factors are responsible for the fibre orientation distribution. At a low Re, the flow in the channel can be approximately regarded as a simple shear flow, and the fibre orientation depends mainly on the initial orientation. The fibre orientation seems equally possible in all directions because initially the fibre's orientations randomly distribute in the exit of channel. With Re increasing, the flow deviates more from the simple shear flow, the flow velocity gradients make the fibres align with the flow direction. It is reported that in a shear flow a fibre will mainly align with the flow direction with occasional tumbling motion if the fluid inertia is present.[21] Now, the fluid inertia is not considered, but the particle inertia is taken into account. It seems that the particle inertia causes qualitatively the same effect as the fluid inertia does. Gavze and Shapiro[22] observed that the particle inertial might result in qualitatively different behaviours of the particle in a shear flow as compared to the case of Stokes flow. This is an interesting fact and needs further investigation.

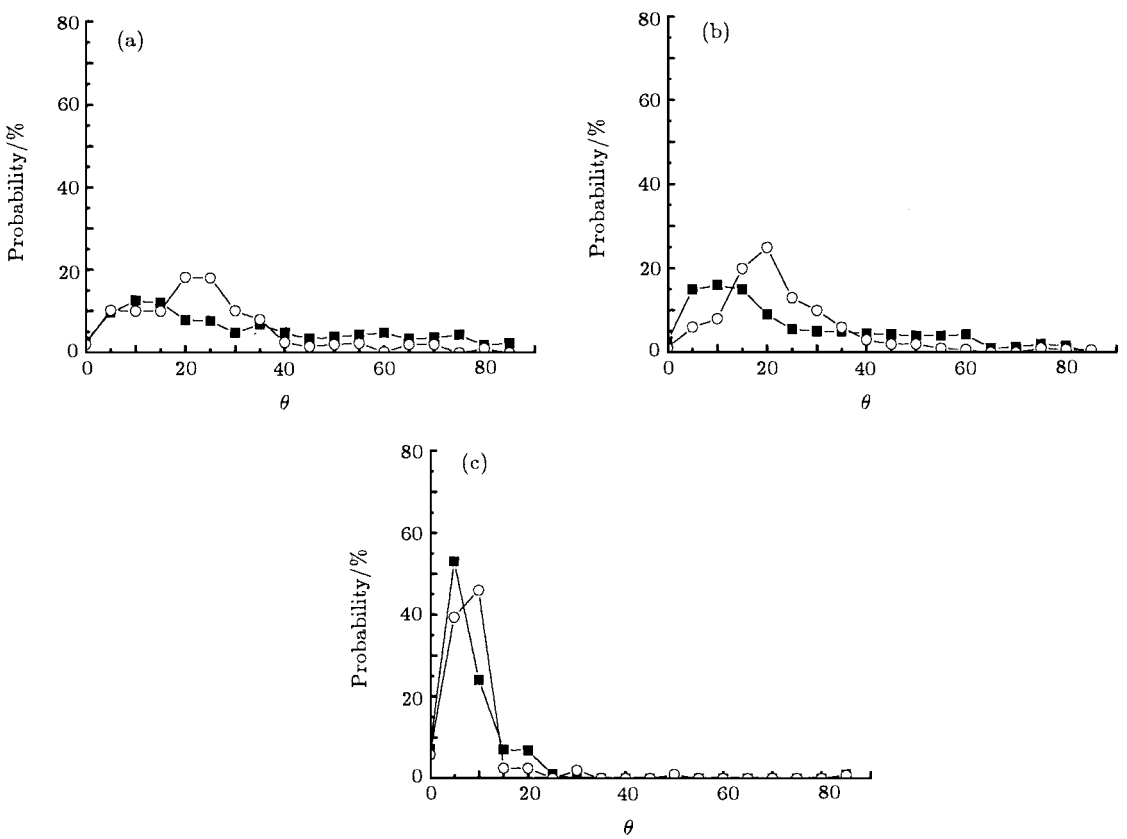


Fig.4. The orientation distribution of fibres for different Re numbers. (a) Re=50, —○—: computation, — ■ —: experiment; (b) Re=100, —○—: computation, — ■ —: experiment; (c) Re=500, —○—: computation, — ■ —: experiment.

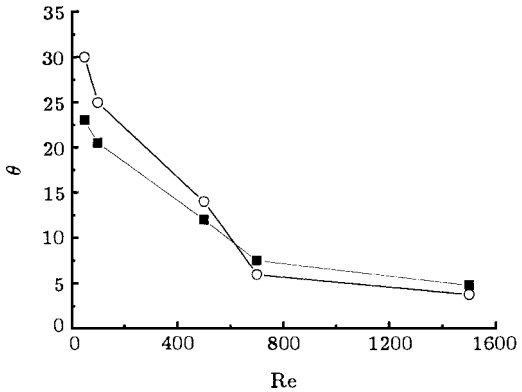


Fig.5. The relationship between Re number and average θ. —◯—: computation; — ■ —: experiment.

4.2. The effect of shear rate of fluid on the orientation distribution of fibres in laminar flows

We divide the cross-section of the channel into four domains as shown in Fig.6, and examine the orientation distributions of fibres in these domains. We analyse the results at two typical Reynolds numbers of 50 and 500. The computational results are shown in Fig.7. We can see that the orientation distribution of fibres narrows more obviously to a low angle as the domain approaches to the wall and the Reynolds numbers increase. Figure 8 shows the average values of θ over each domain at different Reynolds numbers. Similarly, the average value of θ decreases as the domain approaches to the wall and the Reynolds numbers increase. The essential difference among different domains lies in the length scale and shear rate of fluid: the length scale is smaller and the shear rate is higher at a domain approaching to the wall. In our computations, a higher Reynolds number is obtained by increasing the characteristic velocity alone. Figure 9 presents the dimensional shear rates at different domains and different Reynolds numbers, which indicates that the fibres are more aligned with the flow direction at a higher shear rate when other parameters remain unchanged. Therefore, the shear rate is a key dimensionless parameter for the orientation distribution of fibres.

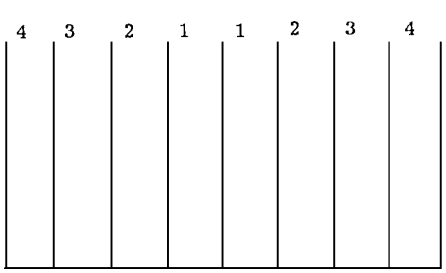


Fig.6. Four domains in the lateral direction of channel.

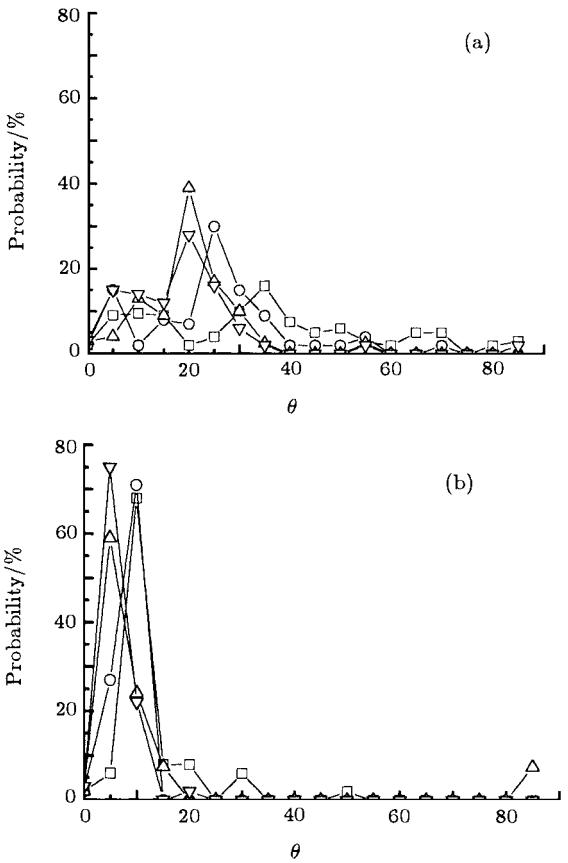


Fig.7. The orientation distributions of fibres in the different domains for. different Re. —□—: Domain 1; —◯—: Domain 2; —△—: Domain 3; —▽—: Domain 4. (a) Re=50; (b) Re=500.

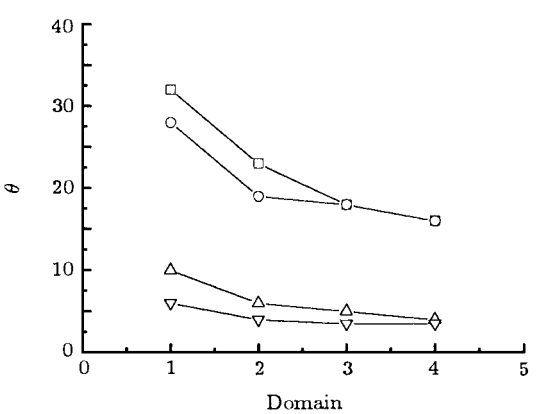


Fig.8. The average angles θ in different domains for different Re. —□—: Re=50; —◯—: Re=100; —△—: Re=500; —▽—: Re=1500.

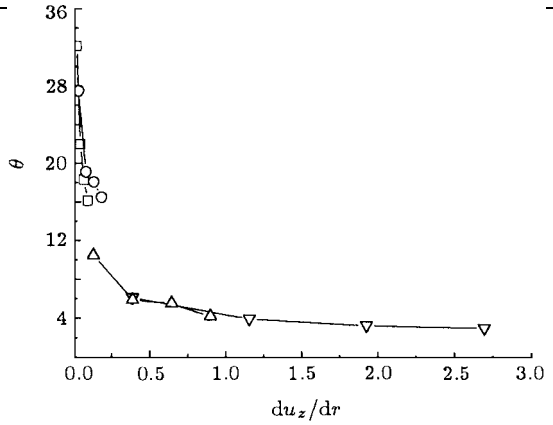


Fig.9. The relationship between average θ and the shear rate of fluid. —□—: Re=50; —○—: Re=100; —△—: Re=500; —▽—: Re=1500.

4.3. The effect of fibre aspect-ratio on the orientation distribution of fibres in the laminar flows

Figure 10 shows the computational orientation distributions of fibres with different aspect-ratios β at Re=500 and Re=700, respectively. It can be found that the difference between the results at different fibre aspect-ratios for both Reynolds numbers is very small. Again based on the theory of Jeffrey orbit, the motion of fibres can be determined by their initial orientation for a simple shear flow. For the fibres with initial randomly-distributed orientations, both the flow velocity gradient and the particle inertia affect the evolution of orientation distribution. At a relatively small Re, e.g. Re=500, the particle inertia plays a greater role in affecting the orientation distribution than the flow velocity gradient does, the orientation distributions are slightly different for different fibre aspect-ratios, as shown in Fig.10(a). For Re=700, the flow velocity gradient has a greater influence on the orientation distribution, the effect of particle inertia is insignificant comparatively, the orientation distributions are not sensitive to the particle inertia and even β, as shown in Fig.10(b). According to the predictions of the Krushkal–Gallily model,[23] for particle's aspect-ratio $\beta > 5$, the orientation is not sensitive to β. Therefore our results are reasonable, since the fibre aspect-ratios in our computations range from 5 to 20.

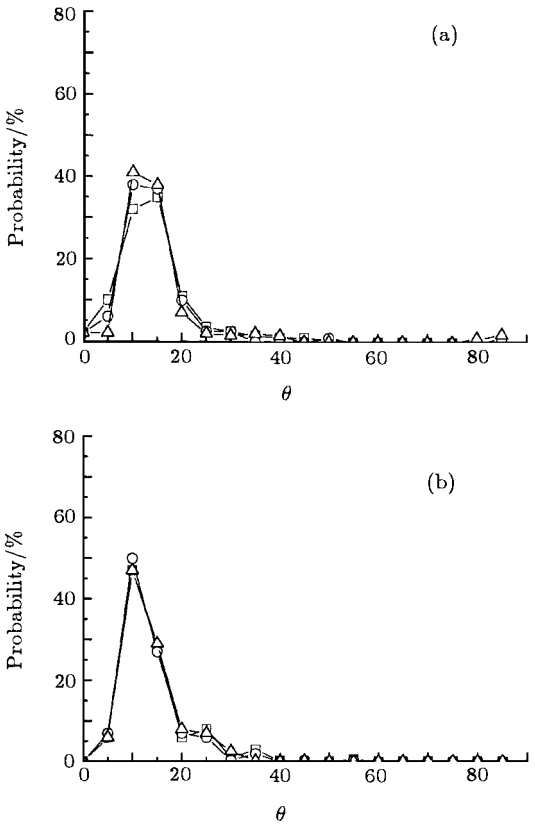


Fig.10. The orientation distributions of fibres with different aspect-ratios for different Re. —□—: β=5; —○—: β=10; —△—: β=20. (a) Re=500; (b) Re=700.

4.4. The effect of fibre density on the orientation distribution of fibres in the laminar flows

Figure 11 is the orientation distributions of fibres with different densities ρ_p at two Reynolds numbers. It is seen that for the fibre density in the given range, the density almost has no influence on the orientation distribution for the two Reynolds numbers. The reason is that the Stokes numbers are very small over the above range of the fibre density. The Stokes number correspondingly changes from 0.00005 to 0.0002 as the fibre density changes from 2000 to 8000kg/m^3. The orientation behaviours of the fibres are not different substantially at such low Stokes numbers.

Therefore, we can conclude that the flow shear rate, or the length scale of flow, has a pronounced effect on the orientation distribution of fibres, whereas the effects of the fibres aspect-ratio and the fibre density are negligible.

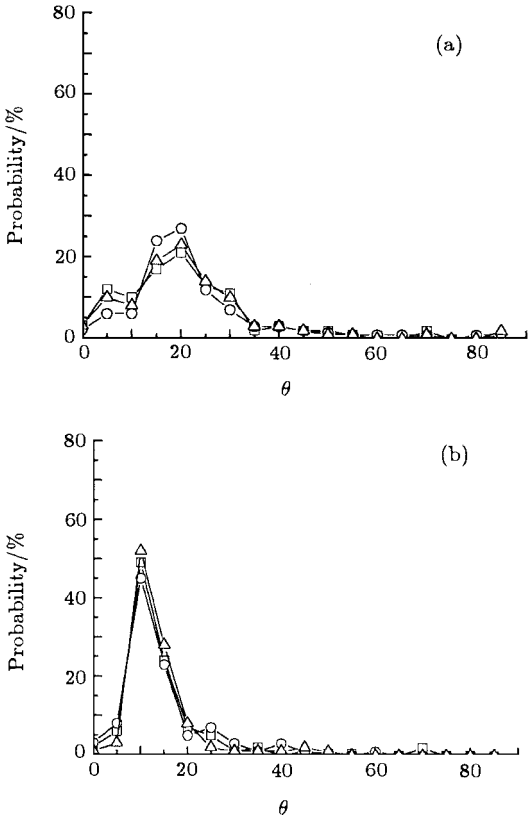


Fig.11. The orientation distributions of fibres with different fibre densities. —□—: ρ_p=2000kg/m^3; —○—: ρ_p=5000kg/m^3; —△—: ρ_p=8000kg/m^3. (a) Re=500; (b) Re=700.

4.5. The fibre concentration in the direction of the channel width in laminar flows

Figure 12 shows the fibre concentration distributions for Re=100. In the computation, we divide the half of channel width $0 \leq (H-r)/H \leq 1$ into eight subregions, their width is the same in the lateral direction. The concentration is represented in terms of the ratio of n to N, where N is the total number of fibres within the assigned region, and n the number of fibres in each subregion. In the figure, the experimental results measured by Yasuda *et al*[8] are also given. Both results are agreeable and show that the fibre concentration distribution is nearly constant though it is low near the side wall. The low fibre concentration near the side wall is due to being exclusive of the force caused by wall.

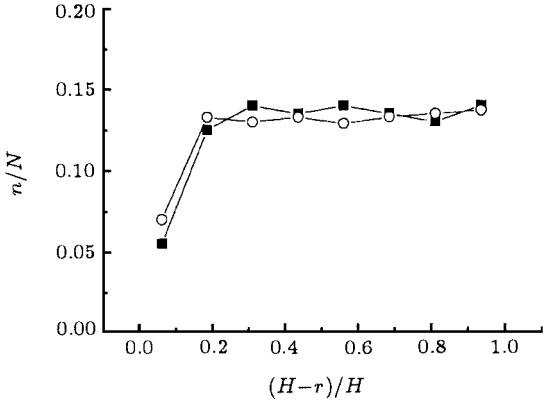


Fig.12. The concentration distributions of fibres in the lateral direction of channel at Re=100. —○—: computation; — ■ —: experiment.

4.6. The effect of turbulence on the orientation distribution of fibres

Here, we compute the motion of fibres in turbulent channel flows with the parameters similar to those used in the Bernstein's experiment and compare the computational results with the experimental results in Fig.13. In the channel flows, the critical Reynolds number from a laminar to turbulent flow is 700–800, and the turbulence is fully developed when Reynolds number is larger than 10000. Figure 13 gives the results for Re=1600 and Re=11000. From the figure, we can see a pronounced influence of turbulence on fibre orientation distribution. At the early transition from a laminar to turbulent flow and Re=1600, the fibres' alignment with the flow direction is obvious. As flow transfers from a laminar to turbulent flow and Re=11000, the turbulences on micro-scales in the different directions become closer, the fibre orientation distribution becomes less concentrated. The reason is that the random fluctuating velocity gradient causes the irregular rotation of fibres and gives rise to the dispersion of the fibre orientation distribution. This dispersive effect is enhanced with Re increasing. Our results are in good agreement with the measurements, indicating that our computational model grasps the physical essence of the fibre motion in turbulence.

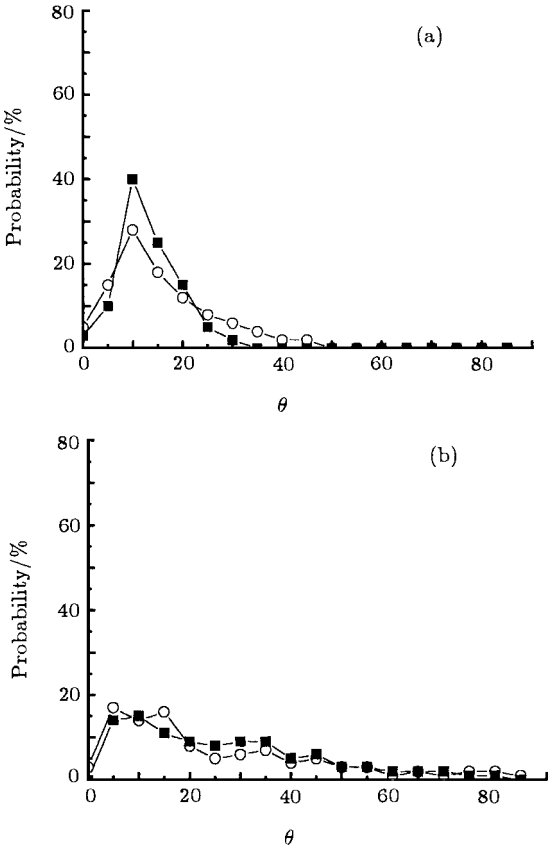


Fig.13. The effect of turbulence on the orientation distribution of fibres. (a) Re=1600, —○—: computation, — ■ —: experiment; (b) Re=11000, —○—: computation, — ■ —: experiment.

4.7. The translational velocity, angular velocity and position diffusion of fibres

The translational and angular velocity components of fibres are calculated. It is obvious that all velocity components fluctuate around their mean value, showing the strong flowing ability of the fibres with the local flow. Naturally, the dimensional velocity fluctuations increase with Reynolds number increasing, for a higher Reynolds number means a higher main stream velocity.

The standard deviations of fibres' translational velocity and angular velocity are defined by

$$u_z'' = \sqrt{\frac{\sum_{n=1}^{N}(u_{nz} - \bar{u}_z)^2}{N}},$$

$$u_r'' = \sqrt{\frac{\sum_{n=1}^{N}(u_{nr} - \bar{u}_r)^2}{N}},$$

$$\omega'' = \sqrt{\frac{\sum_{n=1}^{N}(\omega_n - \bar{\omega})^2}{N}}, \tag{10}$$

where N is the number of fibres. Figures 14, 15 show the relationships between the standard deviations and Reynolds number, respectively. It is found that the standard deviations of fibres' translational velocity and angular velocity increase with the increase of Re. The fluctuating intensity of the translational velocity in the flow direction is stronger than that in the lateral direction.

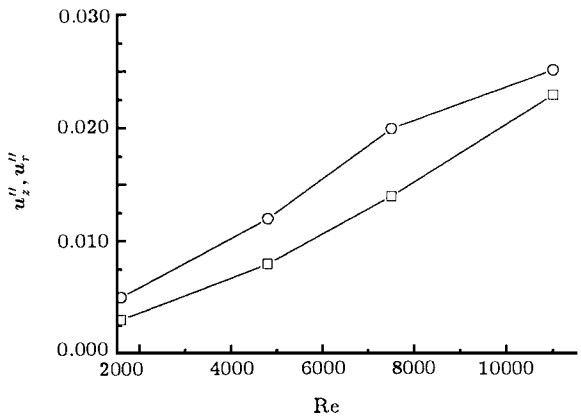


Fig.14. Relationships between Re and the standard deviation of translational velocity of fibre. —○—: u_z''; —□—: u_r''.

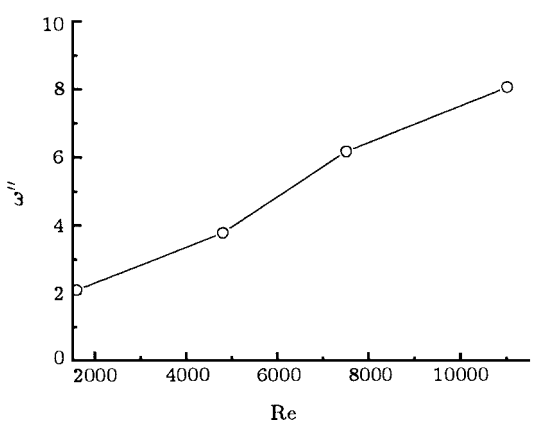


Fig.15. Relationships between Re and the standard deviation of angular velocity of fibre.

In addition, Figure 16 shows fibres' concentration in the lateral direction at Re=11000. The distribution of fibres is similar to that in the case of laminar flow as shown in Fig.12 except that in the region near the wall. The fibre concentration distribution is nearly constant, which is consistent with the experimental results given by Yasuda *et al.*[7] It also can be seen

that more fibres move to the wall in the case of turbulence than laminar flow. This phenomenon conforms to the velocity profiles of laminar flow and turbulence.

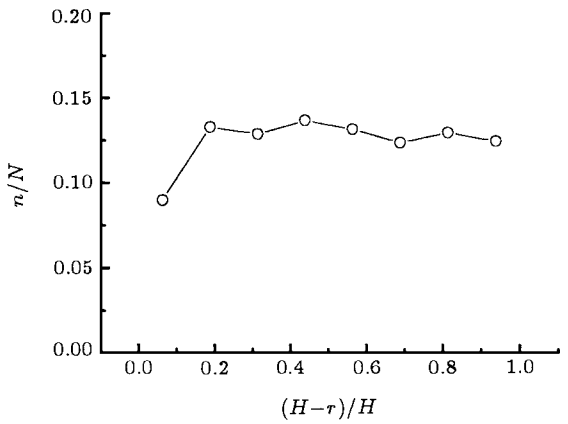


Fig.16. The concentration distribution of fibres in the lateral direction of channel at Re=11000.

5. Conclusion

The orientation and concentration distributions of fibres in laminar and turbulent channel flows are simulated numerically. The simulated results are consistent with the experimental data available in the literature and show that the flow field regime exerts a remarkably strong effect on the orientation distribution of fibres. In the laminar flow regime, more fibres are aligned with the flow direction with the increase of Reynolds number. The shear rate of fluid around a fibre and the length scale of flow are the key factors for determining the orientation distribution of fibres, while the fibre aspect-ratio and the fibre density have a marginal influence on the orientation distribution of fibres. Therefore, it is reasonable to assume the fibres to be inertialess in the paper. In the turbulent regime, the orientation and concentration distributions become more homogeneous with Reynolds number increasing, and the fluctuating intensity of fibre velocity in the downstream direction is larger than that in the lateral direction. More fibres move to the wall in the case of turbulence than in the case of laminar flow.

References

[1] Rosato A D 2000 An Overview of Particle Technology (Singapore: International Publishers Direct) p98
[2] Fan X J, Phan-Thien N and Zheng R 1998 *J. Non-Newtonian Fluid Mech.* **74** 113
[3] Feng J and Leal L G 1997 *J. Rheol.* **41** 1317
[4] Lin J Z, Shi X and Yu Z S 2003 *Int. J. Multiphase Flow* **29** 1355
[5] Guo W B, Shi B C, Wang N C and Guo Z L 2003 *Chin. Phys.* **12** 67
[6] Nsom B 1994 *Fluid Dynam. Res.* **14** 275
[7] Chiba K, Yasuda K and Nakamura K 2001 *J. Non-Newtonian Fluid Mech.* **99** 145
[8] Yasuda K, Mori N and Nakamura K 2002 *Int. J. Eng. Sci.* **40** 1037
[9] You Z J, Lin J Z and Zhang W F 2004 *Fluid Dynam. Res.* **34** 251
[10] Olson J A, Frigaard I, Chan C and Hamalainen J P 2004 *Int. J. Multiphase Flow* **30** 51
[11] Wang L P and Stock D E 1994 *ASME J. Fluid Eng.* **116** 154
[12] Fung J C H, Hunt J C R, Malik N A and Perkins R J 1992 *J. Fluid Mech.* **236** 281
[13] Comte-Bellot G 1965 *Ecoulement turbulent entre des sparois parallels* (Dordrecht: Kluwer) p125
[14] Zhao H P, Liu Z Y and Liu Y Y 2001*Chin. Phys.* **10** 35
[15] Zhao X P and Gao D J 2001 *Acta Phys. Sin.* **50** 1115 (in Chinese)
[16] Li H B and Fang H P 2004 *Chin. Phys.* **13** 2087
[17] Batchelor G K 1979 *J. Fluid Mech.* **44** 419
[18] Happel J and Brenner H 1965 *Low Reynolds Number Hydrodynamics* (Dordrecht: Kluwer) p36
[19] Mackaplow M B and Shaqfeh E S G 1998*J. Fluid Mech.* **376** 149
[20] Bernstein O and Shapiro M 1994 *J. Aerosol Sci.* **25** 113
[21] Karnis A, Goldsmith H L and Mason S G 1966 *Canadian Journal of Chemical Engineering* **44** 181
[22] Gavze E and Shapiro M 1998 *J. Fluid Mech.* **37** 59
[23] Krushkal E M and Gallily I 1998 *J. Aerosol Sci.* **19** 197